Myeloid SHP2 attenuates myocardial ischemia-reperfusion injury via regulation of BRD4/SYK/STING/NOX4/NLRP3 signaling

YAZHONG LIU, HONGSHAN YIN, TAO WANG, TAO CHEN, CHENGDA GUO, FUE ZHANG and ZHIAN JIANG

Department of Cardiovascular Disease and Surgery, Third Hospital of Hebei Medical University, Shijiazhuang, Hebei 050051, P.R. China

Received August 16, 2024; Accepted January 17, 2025

DOI: 10.3892/mmr.2025.13520

Abstract. The objective of the present study was to investigate the impact of myeloid Src homology region 2-containing protein tyrosine phosphatase 2 (SHP2) on myocardial ischemia reperfusion (MI/R) injury and the underlying mechanism. Bioinformatics was used to analyze genes specifically associated with MI/R. In addition, myeloid-specific SHP2 knockout mice and wild-type mice were subjected to MI/R or sham surgery. Echocardiography and Masson's staining were used to observe the myocardial function and infarct area of the mice. In addition, double immunofluorescence staining was used to detect the relative fluorescence intensity of SHP2 and bromodomain-containing protein 4 (BRD4) in bone marrow-derived macrophages (BMMs) from the mice. Western blot analysis was conducted to determine the expression levels of SHP2, BRD4, spleen tyrosine kinase (SYK), stimulator of interferon genes (STING), NADPH oxidase 4 (NOX4), NLR family pyrin domain containing 3 (NLRP3), IL-1β and gasdermin D (GSDMD) in BMMs and mouse myocardial cells co-cultured with the BMMs. In addition, flow cytometry was employed to assess myocardial cell apoptosis. Bioinformatics analysis revealed the downregulated expression of SHP2 and upregulated expression of BRD4 and SYK in mice with MI/R. The deletion of myeloid SHP2 aggravated MI/R injury, impaired cardiac function and increased the infarct area in mice. In addition, myeloid SHP2 deletion in BMMs promoted the expression of BRD4, SYK, STING, NOX4 and NLRP3 in BMMs, and the expression of IL-1β and GSDMD in mouse myocardial cells co-cultured with the BMMs. In addition, the deletion of myeloid SHP2 promoted cardiomyocyte apoptosis. These results indicate that myeloid SHP2 inhibits MI/R injury by regulating BRD4/SYK/STING/NOX4/NLRP3 signaling in BMMs.

Correspondence to: Dr Zhian Jiang, Department of Cardiovascular Disease and Surgery, Third Hospital of Hebei Medical University, 139 Ziqiang Road, Shijiazhuang, Hebei 050051, P.R. China
E-mail: 36300983@hebmu.edu.cn

Key words: myocardial ischemia/reperfusion, SHP2, BRD4, bone marrow-derived macrophages

Introduction

Acute myocardial infarction (AMI) is the most severe manifestation of coronary artery disease; it results from the acute interruption of myocardial blood flow and leads to ischemic necrosis of the heart muscle. It has a marked impact on global health, affecting >7 million individuals annually. The prevalence of AMI in China is increasing, and the prevalence of AMI in men is higher than that in women. It has been predicted that the number of patients with AMI in China will be >23 million by 2030, and data indicate that AMI is increasingly affecting younger individuals (1,2). Cells do not instantly die after myocardial ischemia, and prompt and efficient myocardial reperfusion can mitigate AMI damage and limit infarct size. However, ischemia-reperfusion (I/R), a process where blood supply returns to tissue after a period of ischemia, can cause myocardial I/R (MI/R), subsequently leading to I/R injury (IRI) and cardiomyocyte death. IRI proceeds via several harmful mechanisms, including inflammation, oxidative stress, excessive intracellular calcium, and the rapid restoration of physiological pH (3). The abrupt reperfusion of an ischemic heart can lead to ventricular arrhythmias, myocardial stunning, microvascular obstruction and fatal M/IR injury. Despite the possibility of additional myocardial injury, reperfusion remains the most important and successful treatment for AMI (4). Thus, the prevention and alleviation of IRI remains a critical issue in clinical practice.

Reactive oxygen species (ROS) are the primary type of free radicals that contribute to M/IR injury. They do this by inducing the opening of mitochondrial permeability transition pores, serving as chemoattractants for neutrophils, and causing the sarcoplasmic reticulum to become dysfunctional (5). In addition, ROS facilitate intracellular calcium overload, damage the myocardial cell membrane through lipid peroxidation, induce enzyme denaturation, cause direct oxidative damage to DNA, and ultimately lead to the apoptosis of cardiomyocytes. Therefore, managing the microenvironment of the damaged myocardium by clearing away excess ROS is crucial for the effective treatment of IRI (6). In the myocardium affected by IRI, recruited and activated macrophages serve as reservoirs that generate and release large amounts of ROS into the microenvironment, directly exerting cytotoxic effects on cardiomyocytes (7).

Bromodomain-containing protein 4 (BRD4), a member of the bromodomain and extra-terminal (BET) protein family,

functions as a sensor for ROS. It is crucial for controlling the cell cycle, inflammatory reactions and gene transcription, and is associated with a number of age-related conditions, including tumors, diabetes, pulmonary fibrosis, cardiovascular disorders and ischemic brain damage (8,9). Src homology region 2-containing protein tyrosine phosphatase 2 (SHP2) is a non-receptor protein tyrosine phosphatase, extensively distributed in the cytoplasm of mammals. It is a member of the protein tyrosine phosphatase class, encoded by the ptpn11 gene, and contains two Src homology domains. SHP2 plays a crucial role in regulating the oxidative stress response by modulating various signaling pathways that influence cellular reactions to oxidative stress. During MI/R, the regulatory effect of SHP2 controls the extent of cardiomyocyte apoptosis and injury, as it contributes to regulation of the inflammatory response triggered by MI/R. SHP2 has been shown to modulate the expression and release of inflammatory factors through pathways such as the JAK/STAT pathway, thereby regulating the severity of the inflammatory response (10-13). Additionally, SHP2 has been demonstrated to inhibit the activation of MAPK, which regulates the dynamic chromatin targeting of BRD4 (14). Therefore, it is speculated that SHP2 may affect MI/R injury through the BRD4 signaling pathway. Since SHP2 is known to play multiple regulatory roles in MI/R injury, and to affect the extent of myocardial damage by modulating key processes such as oxidative stress, cellular apoptosis and inflammation, the aim of the present study was to further explore the specific mechanisms of SHP2 and its potential in the treatment of MI/R.

Materials and methods

Bioinformatics analysis. GEOquery (version 2.64.2; Bioconductor), limma (version 3.52.2; Bioconductor), ggplot2 (version 3.3.6; https://ggplot2.tidyverse.org/) and ComplexHeatmap (version 2.13.1; https://jokergoo.github.io/ComplexHeatmap/reference/ComplexHeatmap.html) packages were used together with R software (version 4.2.1; R Core Team). The GEOquery software was used to obtain the GSE108940 dataset from the Gene Expression Omnibus (https://www.ncbi.nlm.nih.gov/geo/) database. The impute software (impute 1.0; Bioconductor) was used to impute missing values from the data. The normalizeBetweenArrays function of the limma package was then used to normalize the data, and probes that corresponded to multiple RNAs were eliminated. Only the probe with the greatest signal value was retained for probes that corresponded to the same RNA. The ggplot2 software was used to generate box plots. The data was subjected to principal component analysis (PCA), and the ggplot2 tool was used to visualize the findings. In addition, the ggplot2 tool was used to visualize the findings of differential analysis, with a threshold set at |LogFC|>1 and adjusted P-value (P.adj)<0.05. Row grouping based on Euclidean distance and row normalization were carried out, and the ComplexHeatmap package was used to visualize the results.

ClusterProfiler (version 4.4.4), GOplot (version 1.0.2), ggplot2 (version 3.3.6) and org.Hs.eg.db (ID conversion software) packages were used together with R software (version 4.2.1; R Foundation) to further analyze the GSE108940 dataset, using mouse (*Mus musculus*) as the species for the analysis. The ID conversion software was used to transform the RNA list to Entrez IDs. The clusterProfiler package was used to perform an enrichment analysis, and the GOplot package was used to compute the z-score values for each enrichment item using the supplied numerical data. When selecting gene clusters and pathways with biological significance among the differentially expressed genes, a threshold of P.adj<0.05 was applied. The identified differentially expressed genes were subjected to Gene Ontology (GO) (http://geneontology.org/) and Kyoto Encyclopedia of Genes and Genomes (KEGG) (http://geneontology.org/) pathway enrichment analyses via the ClusterProfiler package. The ggplot2 software was used to visualize the findings of the enrichment analysis.

The following packages were also used with R software (version 4.2.1) to perform correlation analyses: car (version 3.1-0), stats (version 4.2.1) and ggplot2 (version 3.3.6). Considering the type and distribution of the data, Spearman's rank correlation coefficient was used to perform the analysis. Scatter plots for spleen tyrosine kinase (SYK), BRD4, NADPH oxidase 4 (NOX4), TANK binding kinase 1 (TBK1), interferon regulatory factor 3 (IRF3) and NLR family pyrin domain containing 3 (NLRP3) gene co-expression were generated using the ggplot2 package.

Establishment of animal models. Myeloid-specific SHP2 knockout (KO) mice were selected from the offspring of Lyz2-Cre$^{+/-}$ mice and SHP2Flox$^{/+}$C57BL/6 mice using the Cre-LoxP system. The mice were purchased from Henan Skbes Biotechnology Co., Ltd. The 6-week-old male myeloid-specific SHP2 KO mice and wild-type (WT) mice (18±1 g) were kept at 22±2˚C with free access to food and water and a 12-h light/dark cycle and 50% relative humidity. An MI/R model was established in the myeloid-specific SHP2 KO mice and the WT mice. To establish the model, the mice were anesthetized using isoflurane gas (3% for initiation and 1.5% for maintenance). The surgical instruments were sterilized in an autoclave and aseptic technique was followed. A longitudinal incision was made in the left anterior chest skin, and blunt dissection of the subcutaneous tissue was performed. The third and fourth intercostal spaces were identified, and the thoracic cavity was opened. Sterile cotton wool was placed in the thoracic cavity to cover the lung tissue to prevent damage to the lung tissue and potential fatality. The third rib was carefully cut, and the thoracic cavity was gently opened to expose the heart. The pericardium covering the heart surface was carefully removed using forceps to expose the heart and the left anterior descending branch. The heart was gently compressed, and an 8-0 sterile suture was inserted ~1 mm away from the bifurcation point of the left anterior descending branch, running parallel to it. The suture was placed on the surface of the heart with a polytetrafluoroethylene tube tied around it to secure the suture in place. The heart was quickly placed back into the chest, and the mouse was observed to ensure that an appropriate increase (20-50% increase in base frequency) in respiratory rate occurred. In addition, changes in heart rate and the color of the distal ventricular myocardium were monitored to confirm successful ischemia. Following 30 min of ischemia, the ligature was released by untying the suture and removing the polytetrafluoroethylene tube to allow blood flow to be restored to the ischemic area. The restoration of the pale myocardial tissue to a reddish color

indicated successful reperfusion and model establishment. Four groups of mice were established, namely the sham-WT, sham-SHP2^{MAC-KO} [macrophage-knockout (MAC-KO)], model-WT and model-SHP2^{MAC-KO} groups (each n=6 mice). The mice in the sham groups underwent thoracotomy under anesthesia without any further treatment. The experiment was approved by the Animal Ethics Committee of Hebei North College (Zhangjiakou, China; approval no. 20230610112) and followed the 3R principles.

Echocardiographic assessment of mouse hearts. Echocardiography was performed on all mice in each group 4 weeks after model establishment. An ultrasound probe was used at a frequency of 10 MHz, with adjustment of the scanning speed and image depth to obtain clear images. The mice were anesthetized by the inhalation of 3% isoflurane gas for induction and 1.5% isoflurane to maintain anesthesia. When anesthetized, the mice were secured on a temperature-controlled platform in a supine position. The body was slightly tilted to the left. After ensuring stable breathing and a regular heart rate, the ultrasound probe was gently placed on the left side of the sternum, with a slight adjustment in the direction of the probe to obtain a clear long-axis view of the left ventricle. M-mode ultrasound was used to visualize the motion of the left ventricle. The following data were recorded: Left ventricular internal diameter at end-diastole (LVIDd), LVID at end-systole (LVIDs), left ventricular anterior wall thickness at end-diastole (LVAWd), LVAW at end-systole (LVAWs), ejection fraction (EF) and fractional shortening (FS).

Euthanasia and slice production. Each mouse was placed into an individually ventilated cage, which was then covered securely prior to euthanasia. The cage was filled with CO_2 at a displacement rate of 30-70% of the volume/min. After confirming that the mouse was motionless, not breathing and had dilated pupils, the CO_2 flow was discontinued and the mouse observed for another 2 min to confirm death. The heart was collected, rinsed free of blood with iced saline, and then transferred to a sterile Eppendorf tube and fixed by immersion in 4% paraformaldehyde solution. The fixed tissue was trimmed and then dehydrated using 80, 90, 95 and 100% alcohol concentration gradients. The dehydrated tissues were rendered transparent by treatment with 100% alcohol for 30 min, benzyl alcohol for 10 min, xylene I for 10 min and xylene II for 10 min, and then soaked in paraffin wax for ≥1 h at 60˚C. The paraffin-embedded tissues were sectioned to a thickness of 4-5 μm using a microtome. Sections were transferred to distilled water at 40˚C for spreading, and then mounted onto carrier slices using a cotton swab. After labeling and numbering, the sections were dried in a thermostat.

Masson's staining. Tissues were fixed in 4% paraformaldehyde at 4˚C for 24 h, routinely dehydrated and embedded. Sections (thickness, 4 μm) were dewaxed and rehydrated. The sections were incubated in the staining solution overnight at room temperature, followed by rinsing with running water for 10 min. Nuclei were stained using Regaud's hematoxylin staining solution for 10 min, and after staining, the nuclei were rinsed briefly (10-15 sec) with distilled water. Differentiation was performed using acidic ethanol followed by rinsing with distilled water to stop differentiation. Next, the nuclei were stained with Lichun red compound acidic compound red solution for 10 min, then washed with 2% glacial acetic acid aqueous solution for a few moments, treated with phosphomolybdic acid solution for ~5 min and then washed with 0.2% glacial acetic acid aqueous solution for 1 min. Staining was then performed with aniline blue for 2 min, before washing with 0.2% glacial acetic acid aqueous solution for 1 min. Afterwards, dehydration was performed first with 95% ethanol and then with anhydrous ethanol, before clearing with xylene and mounting with neutral gum. Results were observed using a light microscope. The fibrosis area was then calculated using imageJ (National Institutes of Health).

Cell culture and grouping. Myeloid-specific SHP2 KO mice and WT mice were euthanized, and their bone marrow-derived macrophages (BMMs) were collected. In brief, the femurs and tibias were isolated, cleaned of adherent muscle tissue and washed with 9% physiological saline. The bone ends were cut off to expose the bone marrow cavity, which was washed with physiological saline. The bone marrow flush was filtered through a 70-μm cell filter, and the resulting filtrate was centrifuged at 300 x g for 5 min at room temperature. After discarding the supernatant, the cell pellet was treated with red blood cell lysis buffer (ACK Lysing Buffer; Thermo Fisher Scientific). Following lysis, the suspension was centrifuged at 200 x g for 5 min at room temperature, and the supernatant was discarded.

The lysed cell pellet was resuspended in complete culture medium containing (cat. no. 11875093; Thermo Fisher Scientific, Inc.) macrophage colony-stimulating factor (M-CSF) (cat. no. P6015; Beyotime Institute of Biotechnology) and seeded into a 12-well cell culture plate. The medium was supplemented with 10% fetal bovine serum and 1% penicillin-streptomycin solution. The cells were cultured in the M-CSF-containing complete culture medium, with a change of medium every 2 days. After 6 days, the BMMs had differentiated into mature macrophages and were used for subsequent experiments.

BMMs in the logarithmic growth phase were transfected with BRD4 overexpression vector (BRD4-mimic) or a BRD4 short hairpin RNA (shRNA)-carrying vector using Lipofectamine® 2000 (Thermo Fisher Scientific, Inc.) according to the manufacturer's instructions. The sequence of the BRD4-shRNA was 5'-AACAATTTGTAAACATAG T-3' BRD4-shRNA, and HBLV-U6-Scramble-ZsGreen-Puro (Hanbio Biotechnology Co.) was used as the vector backbone. BMMs from the myeloid-specific SHP2 KO group were cultured in a low-sugar, low-serum (3% FBS) medium (cat. no. 11054020; Thermo Fisher Scientific, Inc.) with 1% O_2 to model the I/R environment. The following BMM groups were established: WT (transfected with empty vector), KO, model-WT, model-KO, model-WT + BRD4-shRNA, model-KO + BRD4-shRNA, model-WT + BRD4-mimic and model-KO + BRD4-mimic.

The HL-1 mouse cardiomyocyte cell line was purchased from Wuhan Procell Life Technology Co., Ltd. These cells were cultivated in DMEM (cat. no. 11320033; Thermo Fisher Scientific, Inc.) supplemented with 1% penicillin-streptomycin solution (cat. no. 15140122; Thermo Fisher Scientific, Inc.) and

10% fetal bovine serum (cat. no. A5670701; Thermo Fisher Scientific, Inc.). A co-culture system comprising HL-1 cells and BMMs was established. The co-culture was performed using a Transwell system to physically separate the HL-1 cells from the BMMs and to exchange signaling molecules through the co-culture substrate for indirect cell-cell interactions. The ratio of HL-1 cells to BMMs was 1:1, and 50,000 cells were inoculated per well. The co-culture was performed at 37˚C, and subsequent experiments were performed after 48 h of co-culture.

Reverse transcription-quantitative PCR (RT-qPCR). Total RNA was extracted from tissues and cells using TRIzol® reagent (cat. no. 15596026CN; Thermo Fisher Scientific, Inc.). RNA purity and concentration were measured, and cDNA was synthesized using a reverse transcription kit (PrimeScript™ RT reagent Kit; Takara Bio). Genomic DNA removal reaction system: gDNA Eraser, 1 μl; 5X gDNA Eraser Buffer, 2 μl; RNA, 1 μg; RNAse FreeH_2O, replenish to 10. A Pipette gun was used to gently blow the reaction system to mix it well and then incubation was performed at 42˚C for 2 min to remove genomic DNA. The reverse transcription reaction system was configured, with genomic DNA removal on ice. Reverse transcription reaction system product: 10 μl; PrimeScript RT Enzyme MIX I, 1 μl; 5X gDNA Eraser Buffer II, 4 μl; RT Peimer Mix, 1 μl; RNAse FreeH_2O, 4 μl. Reverse transcription was performed at 37˚C for 15 min and 85˚C for 5 sec.

The qPCR amplification system comprised SYBR FAST qPCR Master Mix (cat.no. D7260; Beyotime Institute of Biotechnology) (10 μl), forward primer (10 μmol/l, 0.5 μl), reverse primer (10 μmol/l, 0.5 μl), cDNA template (1 μl) and ddH_2O (8 μl), in a total volume of 20 μl. The reaction conditions were 95˚C for 3 min for initial denaturation, followed by 40 cycles of 95˚C for 5 sec, 56˚C for 10 sec and 72˚C for 25 sec, and a melting curve analysis from 65 to 95˚C. Relative expression levels were calculated using the $2^{-\Delta\Delta Ct}$ method with GAPDH as the reference gene (15).

Primer sequences for the target genes (5'-3') were as follows: SHP2 forward, CTTGGTGAGTGAGTAGAT and reverse, CTTACGGCAGAACATTAG; BRD4 forward, GTG GGAGGAAAGAAACAGGGACA and reverse, AGGAGG AGGATTCGGCTGAGG; GAPDH forward, TCC CTCAAG ATTGTCAGCAA and reverse, AGATCCACAACGGAT ACATT.

Western blot analysis. BMMs and HL-1 cells from each group were collected, and were lysed in pre-chilled RIPA lysis solution (cat. no. P0013B; Betoyime Institute of Biotechnology) (89% RIPA + 10% 10X cocktail + 1% PMSF). After centrifuging the lysates for 20 min at 4˚C and 300 x g, the supernatants were collected. A BCA protein assay kit was used to measure the amount of protein in the supernatants. The proteins (20 μg/lane) were separated using SDS-PAGE (SHP2, SYK, STING, NOX4, IL-1β, GSDMD and GAPDH were used with 10% gels. BRD4 and NLRP3 used 8% gels.) and transferred to PVDF membranes. After blocking for 90 min at room temperature using 5% skimmed milk, the membranes were incubated at 4˚C overnight with primary antibodies targeting SHP2 (cat. no. ab300579; 1:1,000; Abcam), BRD4 (cat. no. ab128874; 1:1,000; Abcam), SYK (cat. no. ab40781; 1:1,000; Abcam), stimulator of interferon genes (STING) (cat. no. ab288157; 1:1,000; Abcam), NOX4 (cat. no. AF1498; 1:1,000; Beyotime Institute of Biotechnology), NLRP3 (cat. no. ab263899; 1:1,000; Abcam), IL-1β (cat. no. ab234437; 1:1,000; Abcam), gasdermin D (GSDMD) (cat. no. ab209845; 1:1,000; Abcam) and GAPDH (cat. no. ab181602; 1:1,000; Abcam). After incubation with the primary antibody, the PVDF membrane was removed from the antibody incubation cassette, immersed in TBST and agitated on a shaker for 10 min. This step was repeated three times. Antibodies were diluted using 5% skimmed milk in TBST, secondary antibodies [Goat anti-rabbit IgG H&L (HRP); cat. no. ab205718; 1:2,000; Abcam] were added and the membranes were incubated for 1 h at room temperature. Finally, an ECL detection kit (cat. no. P0018S; Beyotime Institute of Biotechnology) was used to visualize the protein bands and an imaging system was used to capture images of the bands. Greyscale analysis was performed using GAPDH as a loading control. ImageJ was used to analyze the bands (version 1.8.0; National Institutes of Health).

Immunofluorescence staining. BMMs were washed three times with PBS containing 3% BSA (cat. no. 9998; Cell Signaling Technology) and then fixed using 4% paraformaldehyde in PBS. The sample was fixed at 4˚C for 48 h. The cells were permeabilized by incubation at room temperature for 10 min in PBS containing 0.5% Triton X-100. Following permeabilization, the cells were rinsed 3-6 times, each for 5 min, with PBS containing 3% BSA. Next, the cells were incubated overnight at 4˚C with primary antibodies targeting SHP2 (cat. no. ab131541; 1:100; Abcam) and BRD4 (cat. no. 63759; 1:100; Cell Signaling Technology). After three rounds of washing with PBS containing 0.3% BSA, the cells were incubated with secondary antibodies [Donkey Anti-Rabbit IgG H&L (Alexa Fluor® 647); cat. no. ab150075; 1:200; and Goat anti-mouse IgG H&L (Alexa Fluor® 488); cat. no. ab150113; 1:200; both Abcam] for 1 h at room temperature. After three additional washes with PBS containing 0.3% BSA, the cells were counterstained with DAPI for nuclear visualization. After 15 min of incubation at room temperature, 1X PBS was used for washing twice for 5 min each. Finally, the cells were mounted with 50% glycerol (2 μl) and images captured using a fluorescent microscope. Fluorescence intensity was measured using Image J.

Flow cytometry. HL-1 cells from the co-culture experiment were seeded at a density of $2x10^6$ cells/well in a 6-well plate. After allowing the cells to adhere, they were trypsinized; then the cell suspension and supernatant were collected, mixed and subjected to centrifugation. The sample was centrifuged at 400 x g for 5 min at 4˚C. Following removal of the supernatant, the cells were resuspended in FITC and PI staining solution from an apoptosis detection kit (cat. no. C1062S; Beyotime Institute of Biotechnology) in accordance with the manufacturer's instructions. After culture for 20 min in the dark at room temperature, cell apoptosis was analyzed using flow cytometry (BD FACSCalibur; BD Accuri C6; FlowJo, V10.10; BD Biosciences).

Statistical analysis. The statistical program Prism 9.0 (GraphPad; Dotmatics) was used to analyze the data. Data are

presented as the mean ± standard deviation. For comparisons between two groups, t-tests were used, and for comparisons among multiple groups, two-way analysis of variance followed by Tukey's post hoc test was used. $P<0.05$ was considered to indicate a statistically significant difference.

Results

Bioinformatics analysis. The 12 samples from the GSE108940 dataset comprised a sham group and an I/R group, each containing 6 samples derived from the analysis of mouse heart tissue. Normalized signal intensity (Fig. 1A) demonstrates that the data was appropriately normalized. Marked differences between the two groups were shown by PCA (Fig. 1B). A volcano plot revealed that there were 173 significantly upregulated genes and 157 significantly downregulated genes in the I/R group. Expression of SHP2 was downregulated, and expression of BRD4 and SYK was upregulated in I/R (Fig. 1C). The expression patterns of the 330 differentially expressed genes were visualized using a heatmap (Fig. 1D). The input gene list was converted to Entrez IDs, and the differentially expressed genes were subjected to GO and KEGG analysis. The analysis yielded a bar plot (Fig. 1E), bubble plot (Fig. 1F), chord plot (Fig. 1G) and circle plot (Fig. 1H) for visualizing the biological process (BP), cellular component (CC), molecular function (MF) and KEGG enriched pathways. The analysis revealed the enrichment of pathways including 'TNF signaling pathway', 'rheumatoid arthritis' and 'IL-17 signaling pathway'. There was a significant positive correlation between BRD4 and SYK (Fig. 1I; $P<0.001$), which may suggest a role for BRD4 in regulating immune response and cell proliferation. Although the correlation between BRD4 and NOX4 (Fig. 1J) was not significant ($P=0.342$), this result may still reflect the potential function of BRD4 in oxidative stress response. Further analysis showed that there was also a significant positive correlation ($P<0.001$) between TBK1 and IRF3 (Fig. 1K), suggesting a possible synergistic role of these two molecules in the antiviral immune response. In addition, the positive correlation between IRF3 and NLRP3 (Fig. 1L; $P<0.001$) further supported the key role of IRF3 in the regulation of inflammatory response and cell death.

Effects of myeloid-specific SHP2 KO on cardiac function in M/IR injury in mice. The effect of myeloid-specific SHP2 gene KO on cardiac function and structure during M/IR injury were investigated. RT-qPCR analysis revealed that the relative mRNA expression level of SHP2 in the sham-SHP2^{MAC-KO} group was significantly lower than that in the sham-WT group. In addition, the relative mRNA expression level of SHP2 in the model-SHP2^{MAC-KO} group was significantly lower compared with that in the model-WT group (Fig. S1A). This demonstrates that SHP2 was successfully knocked out. Subsequently, ultrasound results revealed that the sham-WT and sham-SHP2^{MAC-KO} groups did not vary significantly in terms of LVIDd, LVIDs, LVAWd, LVAWs, EF or FS. The model-WT and model-SHP2^{MAC-KO} groups exhibited a substantial increase in LVIDd and LVIDs values, and significant reductions in EF, FS, LVAWd and LVAWs values compared with those of the sham-WT and sham-SHP2^{MAC-KO} groups, respectively. In addition, the model-SHP2^{MAC-KO} group had significantly higher LVIDd and LVIDs values and significantly lower LVAWd, LVAWs, EF and FS values compared with those in the model-WT group (Fig. 2). These findings suggest that the cardiac dysfunction associated with myocardial ischemia-reperfusion damage is exacerbated by myeloid-specific SHP2 deletion.

Effects of myeloid-specific SHP2 KO on myocardial pathological injury in mice. Masson's staining results showed that the sham-WT and sham-SHP2^{MAC-KO} groups had normal cardiac tissue structure, regular cardiomyocyte morphology and a minimal area of myocardial infarction. The model-WT group exhibited nuclear dissolution and fragmentation in some cardiomyocytes, in addition to swollen cardiomyocytes, disorganized myocardial fibers with intervening cavities, the acute infiltration of inflammatory cells around necrotic cardiomyocytes, and an increased infarct area. Compared with the model-WT group, the model-SHP2^{MAC-KO} group exhibited greater cardiomyocyte swelling and myocardial fiber damage, an increased infiltration of acute inflammatory cells, and larger infarct area (Fig. 3). These results indicate that myeloid-specific SHP2 KO exacerbates pathological damage in mouse M/IR injury.

Effects of SHP2 on the BRD4/SYK/STING/NOX4/NLRP3 signaling pathway. Analysis of the BMMs by RT-qPCR showed that the mRNA expression of SHP2 in the KO group was significantly lower than that in the WT group, but no significant difference in the mRNA expression of BRD4 between the KO and WT groups was detected. The mRNA expression of SHP2 in the model-WT group was significantly higher than that in the WT group, but the mRNA expression of SHP2 between the model-KO and KO groups was not significantly different. The mRNA expression of BRD4 in the model-WT and model-KO groups was significantly higher than that in the WT and KO groups, respectively. In the Model-WT and Model-KO cells, transfection with BRD4-shRNA did not induce any significant changes in the mRNA expression of SHP2, while the relative mRNA expression of BRD4 was significantly reduced in both types of cells following BRD4-shRNA transfection, and the significant difference between the WT and KO cells was eliminated. In the Model-WT and Model-KO cells, transfection with BRD4-mimic did not cause any significant changes in the mRNA expression of SHP2, but significantly increased the mRNA expression of BRD4 in both cell types, resulting in no significant difference between the WT and KO cells (Fig. S1B). Western blot examination of the BMMs revealed that the expression of SHP2 in the KO group was significantly lower than that of the WT group, but did not detect any discernible changes in the expression levels of BRD4, SYK, STING, NOX4 or NLRP3 between the KO and WT groups. The expression of SHP2 was significantly higher in the model-WT group than in the WT group, but did not differ significantly between the model-KO and KO groups. The expression levels of BRD4, SYK, STING, NOX4 and NLRP3 in the model-WT and model-KO groups were significantly higher than those in the WT and KO groups, respectively. The expression level of SHP2 in the model-WT and model-KO cells did not significantly change following transfection with BRD4-shRNA, whereas the expression levels of BRD4, SYK,

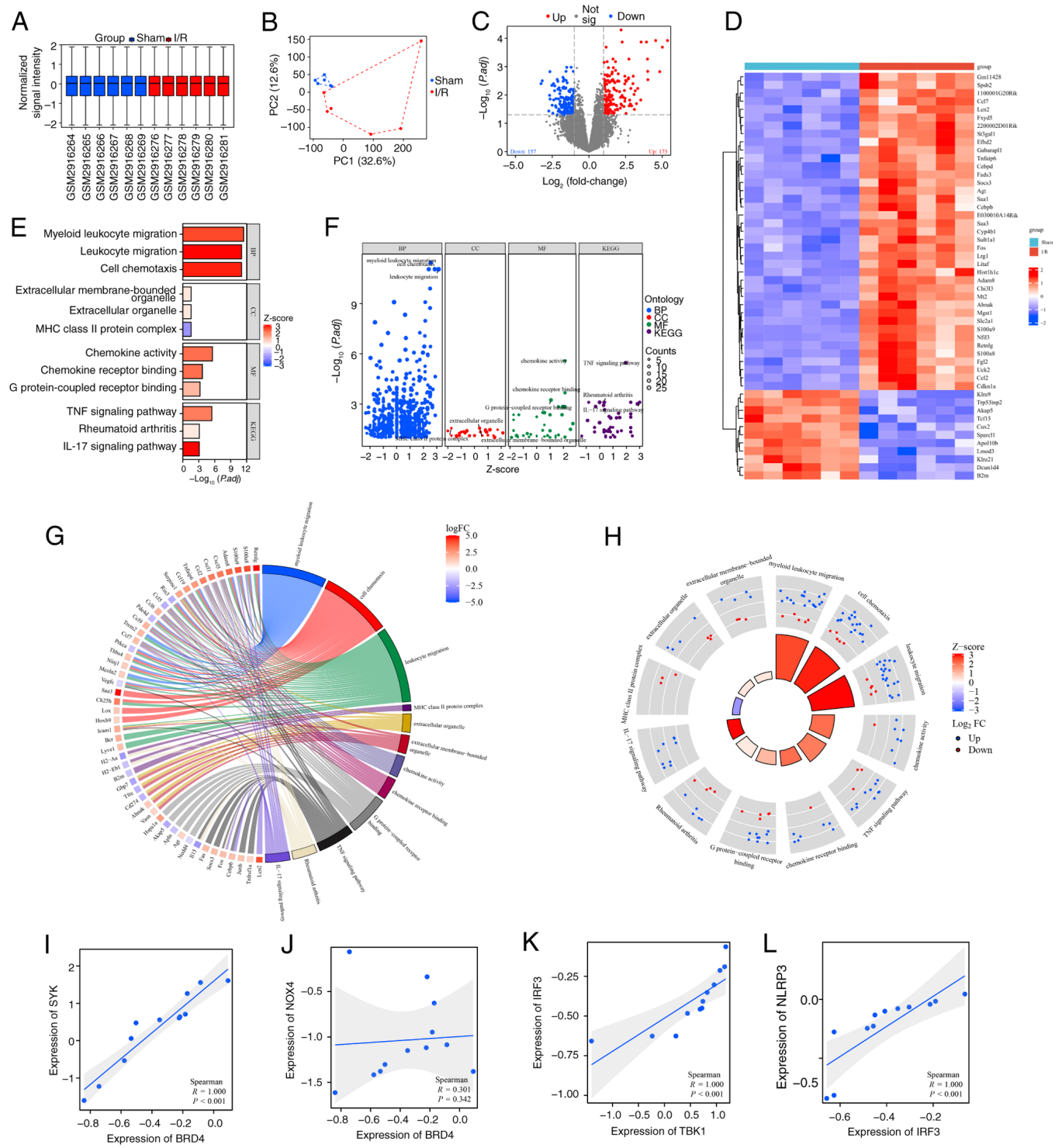

Figure 1. Bioinformatics analysis of the murine GSE108940 dataset. (A) Box plot showing the normalized signal intensity of the samples. (B) Principal component analysis. (C) Volcano plot showing the analysis of differentially expressed genes. (D) Heatmap visualization of the differentially expressed genes in which blue denotes upregulation and green denotes downregulation. (E) Bar, (F) bubble, (G) chord and (H) circle plots visualizing the results of Gene Ontology and KEGG enrichment analysis. Scatter plots showing the correlation of (I) BRD4 and SYK, (J) BRD4 and NOX4, (K) TBK1 and IRF3 and (L) IRF3 and NLRP3. I/R, ischemia reperfusion; PC, principal component; P.adj, adjusted P-value; KEGG, Kyoto Encyclopedia of Genes and Genomes; BP, biological process; CC, cellular component; MF, molecular function; BRD4, bromodomain-containing protein 4; SYK, spleen tyrosine kinase; NOX4, NADPH oxidase 4; TBK1, TANK binding kinase 1; IRF3 interferon regulatory factor 3; NLRP3, NLR family pyrin domain containing 3.

STING, NOX4, and NLRP3 significantly decreased and the significant differences in expression between the WT and KO cells were eliminated. Similarly, the relative protein expression of SHP2 in the model-WT and model-KO cells did not significantly change following transfection with BRD4-mimic, but the expression levels of BRD4, SYK, STING, NOX4 and NLRP3 significantly increased and the significant differences between the WT and KO cells were eliminated.

Immunofluorescence staining of the BMMs revealed that the fluorescence intensity of SHP2 in the KO group was

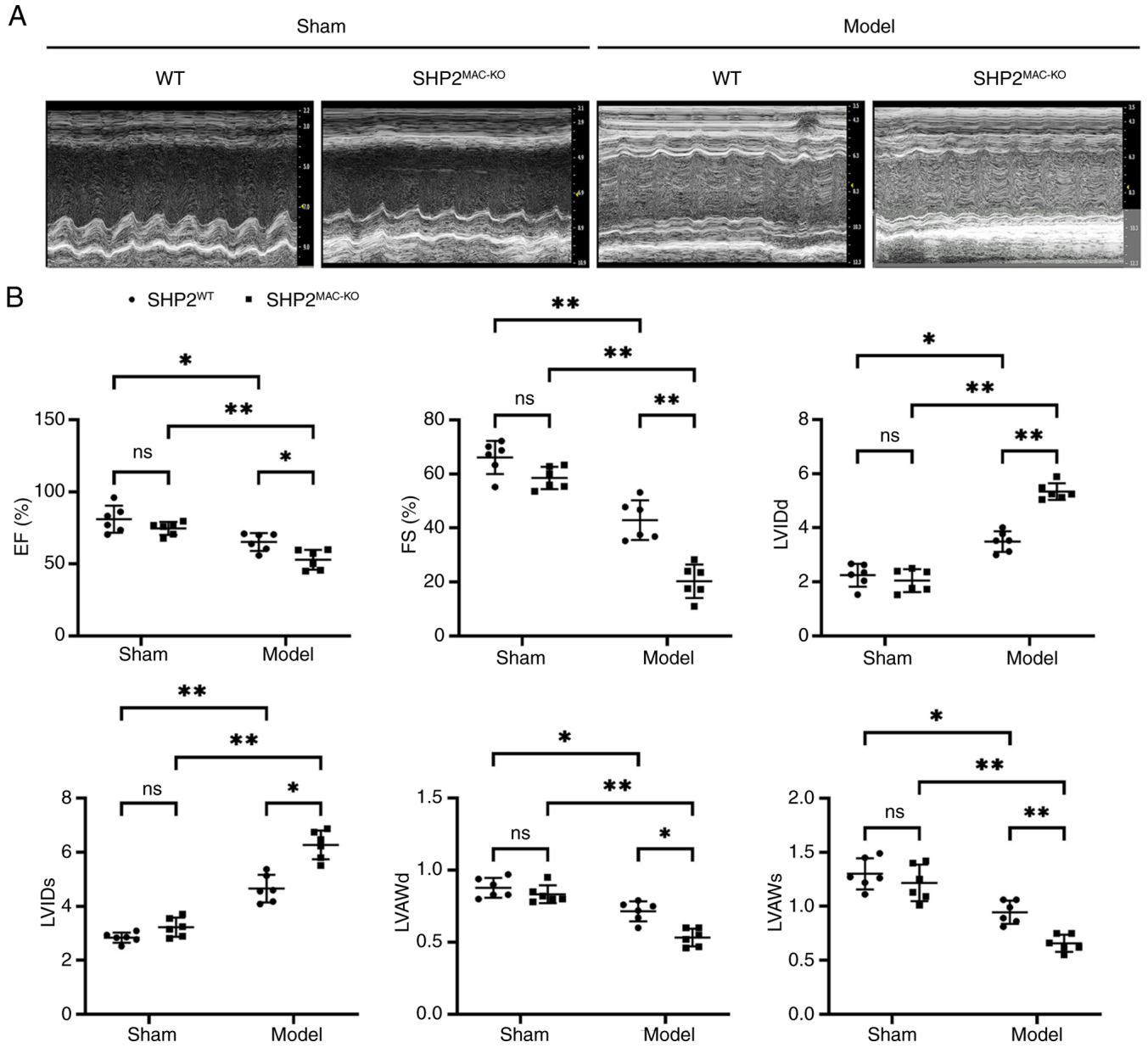

Figure 2. Exacerbation of cardiac dysfunction in myeloid-specific SHP2 KO mice subjected to myocardial ischemia-reperfusion. (A) Ultrasound cardiogram images of mice from the sham-WT, sham-SHP2^{MAC-KO}, model-WT, and model-SHP2^{MAC-KO} groups. (B) Statistical analysis of various echocardiographic parameters in the four groups. Data are expressed as the mean ± standard deviation. *P<0.05 and **P<0.01. ns, not significant; SHP2, Src homology region 2-containing protein tyrosine phosphatase 2; WT, wild type; EF, ejection fraction; FS, fractional shortening; LVIDd, left ventricular internal diameter at end-diastole; LVIDs at end-systole; LVAWd, left ventricular anterior wall thickness at end-diastole; LVAWs, LVAW at end-systole; MAC-KO, macrophage-knockout.

significantly lower than that of the WT group, while there was no discernible difference in the fluorescence intensity of BRD4 between the KO and WT groups. The fluorescence intensity of SHP2 in the model-WT group was significantly higher than that in the WT group, but there was no discernible difference in the fluorescence intensity of SHP2 between the model-KO and KO groups. The fluorescence intensity of BRD4 in the model-WT and model-KO groups was significantly higher than that in the WT and KO groups, respectively (Fig. 4).

Effects of SHP2 on cardiomyocyte apoptosis. Western blotting was used to detect the expression of apoptotic proteins associated with BMMs. Western blotting revealed that the expression levels of IL-1β and GSDMD in the KO group were not significantly from those in the WT group. However, the expression levels of GSDMD and IL-1β in the model-WT and model-KO groups were significantly higher than those in the WT and KO groups, respectively. In addition, the expression levels of GSDMD and IL-1β in the model-KO group were elevated compared with those in the model-WT group. The expression of IL-1β and GSDMD in the model-WT and model-KO groups significantly decreased after transfection with BRD4-shRNA, and the differences between the WT and KO cells were abolished.

Flow cytometry revealed that the HL-1 cells from the KO and WT groups had similarly low apoptotic rates. The apoptotic rates of the cells in the model-WT and model-KO groups was significantly increased compared with those in the WT

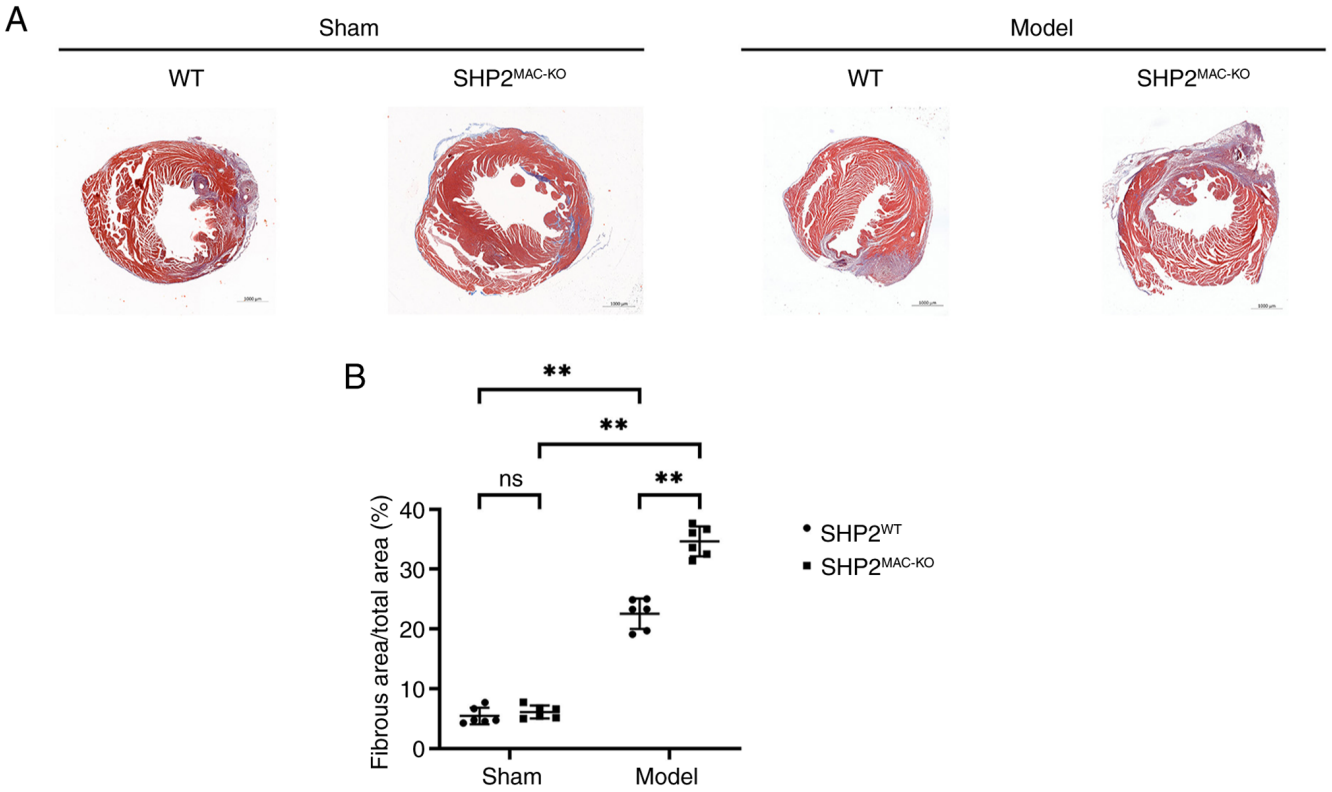

Figure 3. Exacerbation of pathological damage in myeloid-specific SHP2 knockout mice subjected to myocardial ischemia-reperfusion. (A) Masson's staining results showing myocardial tissue sections from the sham-WT, sham-SHP2^{MAC-KO}, model-WT and model-SHP2^{MAC-KO} groups. (B) Comparison of the infarct area in the four groups. Data are expressed as the mean ± standard deviation. **P<0.01. ns, not significant; SHP2, Src homology region 2-containing protein tyrosine phosphatase 2; WT, wild type; KO, knockout

and KO groups, respectively. In addition, the apoptosis rate in the model-KO group was significantly elevated compared with that in the model-WT group. The apoptotic rate of cells in the model-WT and model-KO groups significantly decreased after transfection with BRD4-shRNA, and the difference between the groups was abolished (Fig. 5). These results support the hypothesis that myeloid SHP2 inhibits MI/R injury by regulating BRD4/SYK/STING/NOX4/NLRP3 signaling (Fig. 6).

Discussion

The most effective clinical intervention for myocardial ischemia is prompt reperfusion, which partially restores cardiac function. However, paradoxically, reperfusion can exacerbate cell death and myocardial injury, a phenomenon known as MI/R injury. This triggers excessive ROS production, increased apoptosis and disrupted autophagy, which collectively intensify cardiomyocyte damage and compound myocardial tissue injury. Such effects diminish the therapeutic efficacy of reperfusion and may cause irreversible myocardial damage and increased infarct size (16-18). Addressing MI/R injury remains a key challenge in clinical practice, underscoring the necessity of developing effective strategies for its mitigation.

Macrophages are the most abundant resident leukocytes in the healthy heart. They are the primary inflammatory cells that infiltrate infarcted myocardium and a key source of the pro-inflammatory cytokine IL-1β (19). Previous studies have established an association between SHP2 mutations and congenital cardiovascular disorders (20). In the GSE108940 dataset, data for sham and I/R groups of mice were normalized and significant differences between the two groups were revealed by PCA. Further analysis revealed that there were 173 upregulated and 157 downregulated genes in the I/R group, and a heat map illustrated the expression pattern of 330 differentially expressed genes. Following the conversion of these genes to Entrez IDs, GO and KEGG enrichment analysis was performed and the associated BP, CC, MF and KEGG-enriched pathways were identified. This revealed that these genes were enriched in various terms, including 'TNF signaling pathway', 'rheumatoid arthritis' and 'IL-17 signaling pathway'. In addition, BRD4 expression exhibited a positive correlation with SYK and NOX4 expression, although the latter correlation was not statistically significant. Also, TBK1 expression positively correlated with IRF3, which in turn positively correlated with the expression of NLRP3. In an *in vivo* experiment, the present study found that myeloid-specific SHP2 KO in a mouse model of MI/R suppressed EF, FS, LVAWd, and LVAWs and increased LVIDd and LVIDs. In addition, the myeloid-specific SHP2 KO was observed to increase cardiomyocyte edema and fibrosis, promote the infiltration of acute inflammatory cells, and increase the enlargement of the infarct area. These findings indicate that myeloid-specific SHP2 KO exacerbates the functional and pathological damage caused by MI/R.

BRD4, a member of the BET protein family, plays a pivotal role in cellular senescence, apoptosis, inflammation and gene transcription. Previous research has shown that the downregulation of BRD4 attenuates ischemic brain injury by inhibiting

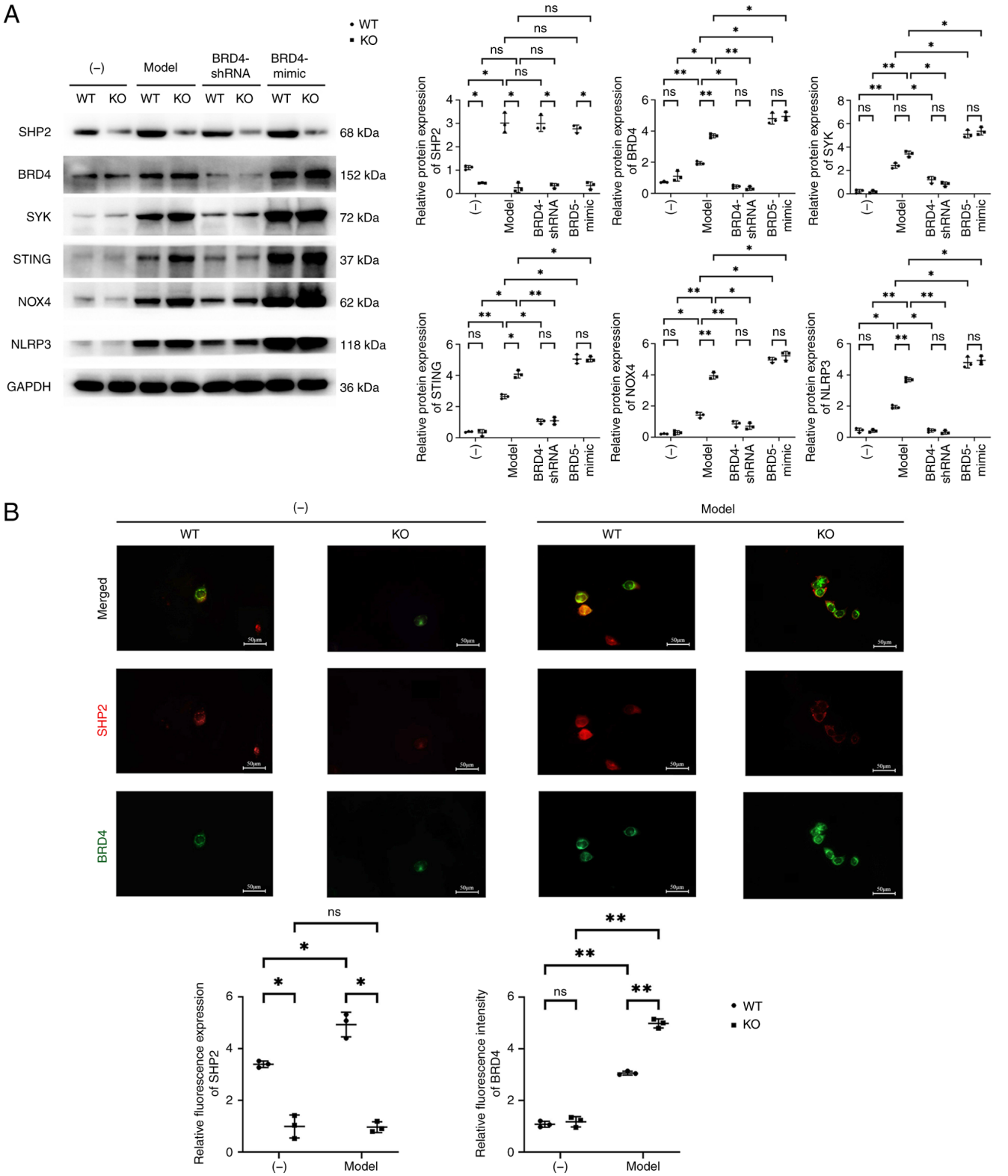

Figure 4. Effects of SHP2 on BRD4/SYK/STING/NOX4/NLRP3 signaling. (A) Representative western blots and quantitative analysis of the relative protein expression levels of SHP2, BRD4, SYK, STING, NOX4 and NLRP3 in murine BMMs, including GAPDH as the loading control. (B) Immunofluorescence staining images and quantitative analysis of the relative fluorescence intensity of SHP2 and BRD4 in the BMMs. Data are expressed as the mean ± standard deviation. *P<0.05 and **P<0.01. ns, not significant; SHP2, Src homology region 2-containing protein tyrosine phosphatase 2; BRD4, bromodomain-containing protein 4; SYK, spleen tyrosine kinase; STING, stimulator of interferon genes; NOX4, NADPH oxidase 4; NLRP3, NLR family pyrin domain containing 3; BMMs, bone marrow-derived macrophages; WT, wild type; KO, knockout; shRNA, short hairpin RNA; mimic, overexpression vector.

inflammation and apoptosis (21). Furthermore, BRD4 suppression delays macrophage senescence via modulation of the NF-κB pathway, thereby decelerating the progression of atherosclerosis. In MI/R injury, the excessive production of ROS disrupts mitochondrial function and damages mitochondrial DNA (mtDNA), aggravating myocardial injury. ROS

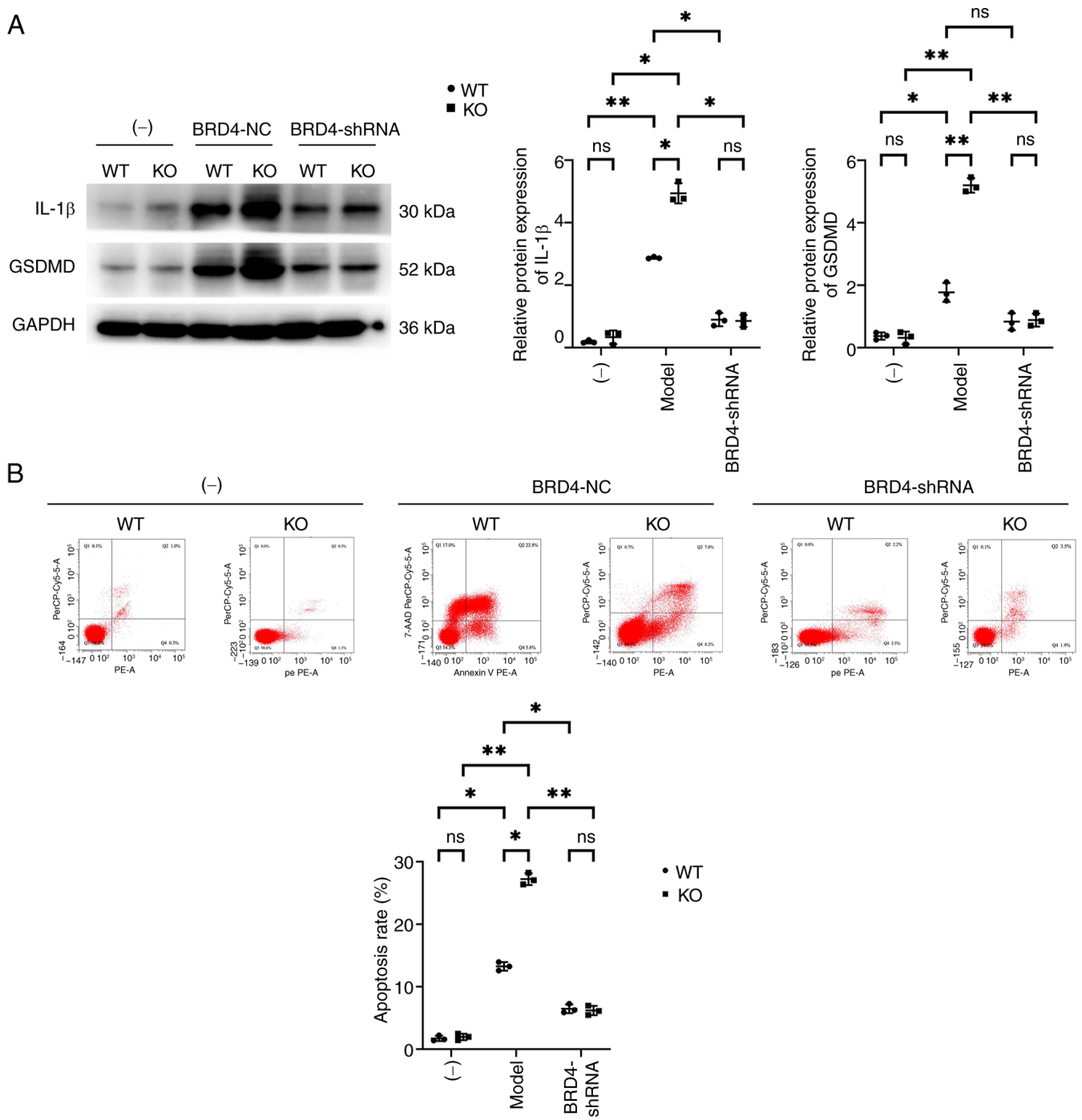

Figure 5. Effects of SHP2 on cardiomyocyte pyroptosis. (A) Representative western blots and quantitative analysis of the relative protein expression levels of IL-1β and GSDMD in BMMs. GAPDH served as the loading control. (B) Flow cytometry analysis of cell apoptosis rates in HL-1 cells. Data are expressed as the mean ± standard deviation. *P<0.05 and **P<0.01. ns, not significant; SHP2, Src homology region 2-containing protein tyrosine phosphatase 2; GSDMD, gasdermin D; BMMs, bone marrow-derived macrophages; WT, wild type; KO, knockout; BRD4, bromodomain-containing protein 4; NC, negative control; shRNA, short hairpin RNA.

also activate BRD4, which upregulates SYK activity and, in turn, increases cyclic GMP-AMP synthase (cGAS) expression, underscoring the role of BRD4 in the regulation of the cGAS pathway (22).

The cGAS/STING signaling pathway is as an important component of the innate immune system. Initially discovered as a cytoplasmic pattern recognition receptor for detecting pathogenic DNA, cGAS was later found to bind to cytosolic free double-stranded DNA, leading to the synthesis of the second messenger cyclic GMP-AMP (cGAMP) from ATP and GTP. The cGAMP interacts with STING, which exists in a homodimeric form on the endoplasmic reticulum, promoting its translocation to perinuclear microsomes. This further activates TBK1, leading to the phosphorylation of STING and providing a binding site for IRF3. In the TBK1-STING-IRF3 complex, TBK1 catalyzes the phosphorylation of IRF3, inducing the secretion of NLRP3 and type I interferon (IFN) family member IFNβ (23,24). SHP2 interacts with TBK1, suppressing its kinase

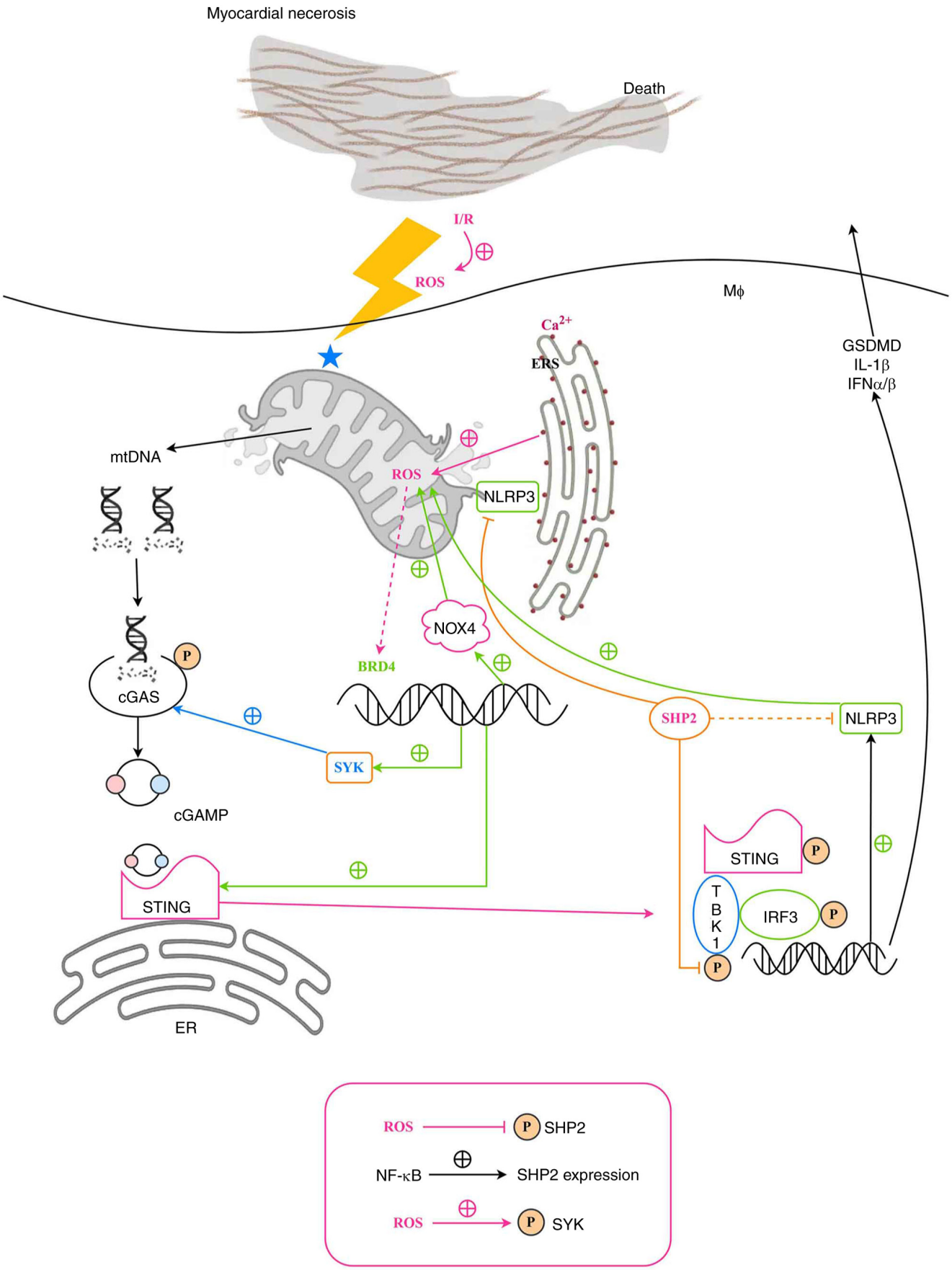

Figure 6. Schematic illustration of the proposed mechanism by which myeloid SHP2 regulates myocardial I/R injury. BRD4, bromodomain-containing protein 4; cGAMP, cyclic GMP-AMP; cGAS, cyclic GMP-AMP synthase; ER, endoplasmic reticulum; ERS, ER stress; GSDMD, gasdermin D; IFN, interferon; I/R, ischemia-reperfusion; IRF3, interferon regulatory factor 3; MØ, macrophage; mtDNA, mitochondrial DNA; NLRP3, NLR family pyrin domain containing 3; NOX4, NADPH oxidase 4; P, phosphorylation; ROS, reactive oxygen species; SHP2, Src homology region 2-containing protein tyrosine phosphatase 2; STING, stimulator of interferon genes; SYK, spleen tyrosine kinase; TBK1, TANK binding kinase 1.

activity via the dephosphorylation of critical residues. In addition, type I interferon synergizes with pro-inflammatory signals such as NF-κB, which amplifies cytokine network responses and indirectly stimulates IL-1β production (25).

NLRP3 is an intracellular pattern recognition receptor that detects pathogenic molecules and endogenous damage signals. Upon activation, NLRP3 forms the inflammasome complex by combining with apoptosis-associated speck-like protein containing a CARD and caspase-1. This complex often assembles at mitochondrial-endoplasmic reticulum contact sites (MERCs), which are microenvironments that facilitate signal transduction (26,27). NLRP3 localizes to mitochondria via interaction with binding partners such as thioredoxin-interacting protein in response to ROS (28). Calcium ion release at MERCs is pivotal in inflammasome activation, capturing calcium signals to initiate downstream pathways. Signal 2 activators recruit SHP2 to mitochondria via its RRWFH motif, with translocation facilitated by Tom20/Tom40 and Tim23 complexes. SHP2 dephosphorylates ANT1 at Tyr191 within the mitochondrial matrix, which regulates mitochondrial homeostasis, mitigating mtDNA leakage and curbing ROS production, thereby dampening NLRP3 inflammasome activation. Thus, SHP2 serves as a negative regulator of the NLRP3 inflammasome (29).

IL-1β is a central pro-inflammatory cytokine that plays a pivotal role in infection and inflammation. Activation of the NLRP3 inflammasome allows caspase-1 to cleave pro-IL-1β into its mature, active form, which is secreted extracellularly to mediate inflammation. The essential pyroptosis effector GSDMD is cleaved by caspase-1 into two fragments: N-terminal fragment GSDMD-N and C-terminal fragment GSDMD-C. The GSDMD-N fragment forms membrane pores that lead to cellular content leakage and pyroptotic cell death, a pro-inflammatory form of programmed cell death. Pyroptosis is characterized by membrane rupture and the release of inflammatory mediators through GSDMD-mediated pores (30,31). The present study revealed that the myeloid-specific KO of SHP2 promoted the expression of BRD4, SYK, STING, NOX4 and NLRP3 in BMMs, as well as IL-1β and GSDMD in HL-1 cells co-cultured with the BMMs, and induced pyroptosis in HL-1 cells. Furthermore, the transfection of BMMs with BRD4-shRNA and BRD4-mimic demonstrated that SHP2 mediates the regulation of the BRD4 signaling pathway in BMMs in response to MI/R injury.

In summary, the present study suggests that myeloid SHP2 inhibits MI/R injury by regulating BRD4/SYK/STING/NOX4/NLRP3 signaling. This implies that molecules in this pathway may serve as new therapeutic targets for the treatment of MI/R injury. In addition, it explored the possibility that SHP2 in the myeloid lineage may provide a comprehensive, multi-level protective mechanism via the simultaneous regulation of multiple signaling pathways, such as those involving BRD4, SYK, STING, NOX4 and NLRP3. This concept of multi-pathway regulation greatly expands the understanding of the pathophysiology of MI/R injury compared with that of traditional single-pathway research, and suggests novel targets for treatment. Furthermore, the concept of combining systemic and local inflammation regulation offers a new perspective for the treatment of IRI. However, numerous studies on SHP2 and the aforementioned signaling pathways have been conducted in animal models, which may limit the extrapolation of research results to human physiological and pathological states. Notably, while mouse models are widely used in the study of cardiovascular disease and immune responses, their immune systems differ from those of humans. Therefore, translating these findings into clinical treatments will require further verification in human studies.

Acknowledgements

The authors acknowledge that due to the complexity of establishing the mouse MI/R model, Mr. Jianchun Fan, a student of Hebei North College (Zhangjiakou, Hebei, China) performed the surgery and provided guidance.

Funding

No funding was received.

Availability of data and materials

The data generated in the present study may be requested from the corresponding author.

Authors' contributions

YL and ZJ were responsible for study concept and design. HY, TW and TC contributed to manuscript writing and the cell experiments. CG and FZ were responsible for the animal experiments. YL and ZJ confirm the authenticity of all the raw data. All authors read and approved the final manuscript.

Ethics approval and consent to participate

This study was approved by the Animal Ethics Committee of Hebei North College (approval number, 20240610112). The Medical Ethics Committee of the Third Hospital of Hebei Medical University was aware of the collaboration with Hebei North College and considered that since Hebei North College had already conducted an ethical review, no additional ethical review was necessary.

Patient consent for publication

Not applicable.

Competing interests

The authors declare that they have no competing interests.

References

1. Xu S, Wu B, Zhong B, Lin L, Ding Y, Jin X, Huang Z, Lin M, Wu H and Xu D: Naringenin alleviates myocardial ischemia/reperfusion injury by regulating the nuclear factor-erythroid factor 2-related factor 2 (Nrf2)/System xc-/glutathione peroxidase 4 (GPX4) axis to inhibit ferroptosis. Bioengineered 12: 10924-10934, 2021.
2. Tian H, Zhao X, Zhang Y and Xia Z: Abnormalities of glucose and lipid metabolism in myocardial ischemia-reperfusion injury. Biomed Pharmacother 163: 114827, 2023.
3. Zhang XJ, Liu X, Hu M, Zhao GJ, Sun D, Cheng X, Xiang H, Huang YP, Tian RF, Shen LJ, *et al*: Pharmacological inhibition of arachidonate 12-lipoxygenase ameliorates myocardial ischemia-reperfusion injury in multiple species. Cell Metab 33: 2059-2075.e10, 2021.

4. Schanze N, Hamad MA, Nührenberg TG, Bode C and Duerschmied D: Platelets in myocardial ischemia/reperfusion injury. Hamostaseologie 43: 110-121, 2023.
5. Bugger H and Pfeil K: Mitochondrial ROS in myocardial ischemia reperfusion and remodeling. Biochim Biophys Acta Mol Basis Dis 1866: 165768, 2020.
6. Shen S, He F, Cheng C, Xu B and Sheng J: Uric acid aggravates myocardial ischemia-reperfusion injury via ROS/NLRP3 pyroptosis pathway. Biomed Pharmacother 133: 110990, 2021.
7. Hao T, Qian M, Zhang Y, Liu Q, Midgley AC, Liu Y, Che Y, Hou J and Zhao Q: An injectable dual-function hydrogel protects against myocardial ischemia/reperfusion injury by modulating ROS/NO disequilibrium. Adv Sci (Weinh) 9: e2105408, 2022.
8. Liu H, Wang L, Weng X, Chen H, Du Y, Diao C, Chen Z and Liu X: Inhibition of Brd4 alleviates renal ischemia/reperfusion injury-induced apoptosis and endoplasmic reticulum stress by blocking FoxO4-mediated oxidative stress. Redox Biol 24: 101195, 2019.
9. Zhu W, Wu RD, Lv YG, Liu YM, Huang H and Xu JQ: BRD4 blockage alleviates pathological cardiac hypertrophy through the suppression of fibrosis and inflammation via reducing ROS generation. Biomed Pharmacother 121: 109368, 2020.
10. Liu M, Fu D, Gao T, Jiang H, Yang P and Li X: The low expression of miR-155 promotes the expression of SHP2 by inhibiting the activation of the ERK1/2 pathway and improves cell pyroptosis induced by I/R in mice. Aging (Albany NY) 16: 4778-4788, 2024.
11. Gao T, Liu M, Fu D, Xue Y, Liao J, Yang P and Li X: Allicin treats myocardial infarction in I/R through the promotion of the SHP2 axis to inhibit p-PERK-mediated oxidative stress. Aging (Albany NY) 16: 5207-5223, 2024.
12. Sha M, Li H, Guo B and Geng X: Myeloid-specific knockout of SHP2 regulates PI3K/PLCγ signaling pathway to protect against early myocardial infarction injury. Aging (Albany NY) 15: 9877-9889, 2023.
13. Lauriol J, Jaffré F and Kontaridis MI: The role of the protein tyrosine phosphatase SHP2 in cardiac development and disease. Semin Cell Dev Biol 37: 73-81, 2015.
14. Stratton MS, Bagchi RA, Felisbino MB, Hirsch RA, Smith HE, Riching AS, Enyart BY, Koch KA, Cavasin MA, Alexanian M, *et al*: Dynamic chromatin targeting of BRD4 stimulates cardiac fibroblast activation. Circ Res 125: 662-677, 2019.
15. Livak KJ and Schmittgen TD: Analysis of relative gene expression data using real-time quantitative PCR and the 2(-Delta Delta C(T)) method. Methods 25: 402-408, 2001.
16. Zhao J, Zhang J, Liu Q, Wang Y, Jin Y, Yang Y, Ni C and Zhang L: Hongjingtian injection protects against myocardial ischemia reperfusion-induced apoptosis by blocking ROS induced autophagic-flux. Biomed Pharmacother 135: 111205, 2021.
17. Li X and Jin Y: Inhibition of miR-182-5p attenuates ROS and protects against myocardial ischemia-reperfusion injury by targeting STK17A. Cell Cycle 21: 1639-1650, 2022.
18. Yu L, Zhang W, Huang C, Liang Q, Bao H, Gong Z, Xu M, Wang Z, Wen M and Cheng X: FoxO4 promotes myocardial ischemia-reperfusion injury: The role of oxidative stress-induced apoptosis. Am J Transl Res 10: 2890-2900, 2018.
19. Francisco J and Del Re DP: Inflammation in myocardial ischemia/reperfusion injury: Underlying mechanisms and therapeutic potential. Antioxidants (Basel) 12: 1944, 2023.
20. Zhou L, Yang S and Zou X: Farrerol alleviates myocardial ischemia/reperfusion injury by targeting macrophages and NLRP3. Front Pharmacol 13: 879232, 2022.
21. Liu L, Yang C, Lavayen BP, Tishko RJ, Larochelle J and Candelario-Jalil E: Targeted BRD4 protein degradation by dBET1 ameliorates acute ischemic brain injury and improves functional outcomes associated with reduced neuroinflammation and oxidative stress and preservation of blood-brain barrier integrity. J Neuroinflammation 19: 168, 2022.
22. Li X, Chen X, Zheng L, Chen M, Zhang Y, Zhu R, Chen J, Gu J, Yin Q, Jiang H, *et al*: Non-canonical STING-PERK pathway dependent epigenetic regulation of vascular endothelial dysfunction via integrating IRF3 and NF-κB in inflammatory response. Acta Pharm Sin B 13: 4765-4784, 2023.
23. Qiao X, Zong Y, Liu Z, Wu Z, Li Y, Wang L and Song L: The cGAS/STING-TBK1-IRF regulatory axis orchestrates a primitive interferon-like antiviral mechanism in oyster. Front Immunol 12: 689783, 2021.
24. Oduro PK, Zheng X, Wei J, Yang Y, Wang Y, Zhang H, Liu E, Gao X, Du M and Wang Q: The cGAS-STING signaling in cardiovascular and metabolic diseases: Future novel target option for pharmacotherapy. Acta Pharm Sin B 12: 50-75, 2022.
25. Zheng Q, Hou J, Zhou Y, Yang Y, Xie B and Cao X: Siglec1 suppresses antiviral innate immune response by inducing TBK1 degradation via the ubiquitin ligase TRIM27. Cell Res 25: 1121-1136, 2015.
26. Tian L, Yu Q, Zhang L and Zhang J: Accelerated fibrosis progression of diabetic nephropathy from high uric acid's activation of the ROS/NLRP3/SHP2 pathway in renal tubular epithelial cells under high glucose conditions. Altern Ther Health Med: June 5, 2024 (Epub ahead of print).
27. Guo W, Liu W, Chen Z, Gu Y, Peng S, Shen L, Shen Y, Wang X, Feng GS, Sun Y and Xu Q: Tyrosine phosphatase SHP2 negatively regulates NLRP3 inflammasome activation via ANT1-dependent mitochondrial homeostasis. Nat Commun 8: 2168, 2017.
28. Lin Q, Li S, Jiang N, Shao X, Zhang M, Jin H, Zhang Z, Shen J, Zhou Y, Zhou W, *et al*: PINK1-parkin pathway of mitophagy protects against contrast-induced acute kidney injury via decreasing mitochondrial ROS and NLRP3 inflammasome activation. Redox Boil 26: 101254, 2019.
29. Qiu Z, He Y, Ming H, Lei S, Leng Y and Xia ZY: Lipopolysaccharide (LPS) aggravates high glucose- and hypoxia/reoxygenation-induced injury through activating ROS-dependent NLRP3 inflammasome-mediated pyroptosis in H9C2 cardiomyocytes. J Diabetes Res 2019: 8151836, 2019.
30. Li S, Sun Y, Song M, Song Y, Fang Y, Zhang Q, Li X, Song N, Ding J, Lu M and Hu G: NLRP3/caspase-1/GSDMD-mediated pyroptosis exerts a crucial role in astrocyte pathological injury in mouse model of depression. JCI Insight 6: e146852, 2021.
31. Coll RC, Schroder K and Pelegrín P: NLRP3 and pyroptosis blockers for treating inflammatory diseases. Trends Pharmacol Sci 43: 653-668, 2022.